Theory and Design of a Hybrid Wave-front Sensor for Adaptive Optics

Charlotte E. Guthery and Michael Hart

College of Optical Sciences, University of Arizona, 1630 E University Blvd, Tucson, AZ, USA

ABSTRACT

Wave-front sensors (WFS) are used in adaptive optics (AO) systems to measure real-time aberrations caused by the atmosphere. The design of a WFS is driven by three desirable parameters: linearity, high sensitivity, and a wide dynamic range. The benefit of the Hybrid WFS (HyWFS) is its wide dynamic range and high sensitivity combined with only a minimally non-linear reconstruction. This is achieved by combining a Shack-Hartmann WFS (SHWFS), which has wide dynamic range, and a Pyramid WFS (PyWFS), which has high sensitivity, into a single system. The first half of the system will resemble a typical PyWFS while the second half includes a lenslet array, typical of a SHWFS. This system will focus portions of the pupils created by the pyramid prism to points on the detector, creating an image of four spot arrays. The output of the HyWFS system has been analyzed in simulations using reconstructors based from slope measurements, raw intensity values, and a combination of the two. These simulations show that, when the applied wave-front error is small, the system benefits from using the PyWFS reconstruction. For larger applied wave-front error the HyWFS can switch to the SHWFS reconstruction, which allows for larger dynamic range than the PyWFS. With this ability to shift, the HyWFS is able to reduce the residual wave-front error by preserving the range and sensitivity without requiring PyWFS modulation or reconstruction.

1. INTRODUCTION

Adaptive optics systems are a necessary feature in the new generation of large aperture telescopes. The resolution capabilities given by a large primary mirror are negated by the turbulence present in the atmosphere. On average, the turbulence limits resolution to 1 arcsecond, while the diffraction limit of large telescopes are orders of magnitude smaller. An adaptive optics system is a powerful tool with the ability to remove the effects of turbulence and restore the diffraction limited imaging capabilities of the system.

Wave-front sensors (WFS) are essential for AO corrections. A system must first measure turbulence before being able to correct it. A wave-front sensor measures the shape of an incoming turbulent wave-front by using a reconstructor matrix to decompose it into a into a set of basis functions. Each wave-front sensor design has specific strengths and weaknesses.

The Shack-Hartmann WFS (SHWFS) is very common type of WFS used for a large variety of applications. The main advantages are a large dynamic range, linear reconstructions, and linear response. This is especially helpful in a highly turbulent medium, where large structural events are not easily predicted. The system uses a lenslet array to image an incoming wave-front into a spot array pattern. In most applications each spot formed by the SHWFS is imaged onto a quad cell on the detector. The change of intensity measured on the quad cell is used to determine the local slope of the wave-front. The drawback of the SHWFS is its limited sensitivity to the low-order aberrations that make up the bulk of the atmospheric wave-front error, an effect attributable to the filtering imposed by the diffraction limit of the lenslet array subapertures.

Other wave-front sensors prioritize a highly sensitive response. Wave-front sensors like the Pyramid WFS (PyWFS) do this by utilizing the entire diffraction limit of the telescope aperture.[1] A PyWFS operates by focusing a beam onto the tip of a pyramid prism. Those in use today typically have four sides, but three sided pyramids have been show to work as effectively.[2,3] The light will split at the prism tip, collimated and imaged onto a detector (Figure 1). The intensity in the resulting pupils gives detailed information about the incoming wave-front with high sensitivity.

The PyWFS generally struggles when it comes to dynamic range. If large turbulence occurs the focused beacon can shift off of the tip of the pyramid prism. This will cause one or more of the pupil images to darken

and the system can no longer measure accurately. PyWFS in practice solve this problem by modulating the focused beam around the tip of the pyramid prism at a frequency that illuminates all pupils in a single exposure.[1] This helps to preserve some of the range of the WFS, but at a loss of overall sensitivity. The dynamic range of the PyWFS is limited by the amplitude of that modulation.

There are a few wave-front sensors in practice that have both a high dynamic range and high sensitivity. Unfortunately those, such as the non-linear curvature WFS, suffer from a non-linear response. This non-linearity becomes an issue as it affects computation times and require a more complex reconstructor.

The driving motivation behind the HyWFS is to create a system with high dynamic range, high sensitivity, and a linear response. To achieve this the HyWFS combines the SHWFS and the PyWFS into a single system. The HyWFS takes advantage of the high dynamic range of the SHWFS and the sensitivity of the PyWFS, combining them into a single WFS with a relatively linear response.

2. HYWFS SENSOR DESIGN

The preliminary design of the HyWFS, shown in Figure 1, combines SHWFS and PyWFS elements. Similar to a PyWFS, the first element of the system is a pyramid prism. This prism takes a focused beam and splits the light into multiple images of the pupil, one for each side of the prism. After the split pupil images are collimated, the system looks identical to a PyWFS.
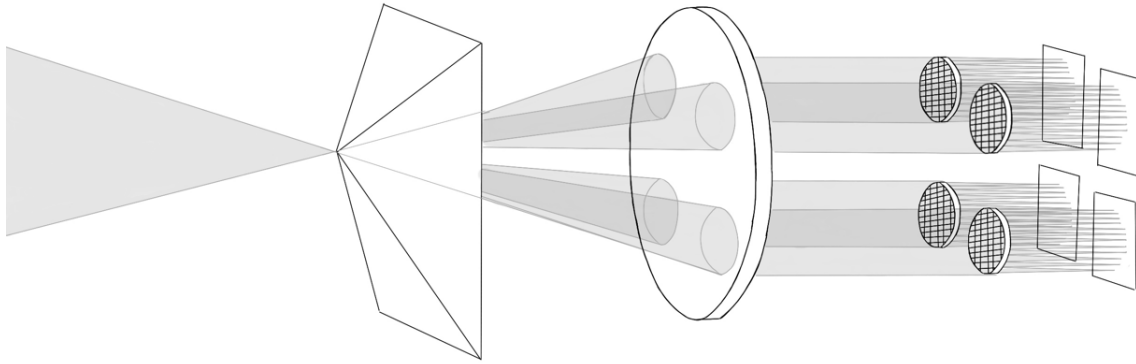

Figure 1. Design of the HyWFS with a four-sided pyramid prism

One novel aspect of the HyWFS is realized by placing a lenslet array before the detector, imaging each of the pupils as a grid of SHWFS spots. In simulation, the system is modeled with a four-sided pyramid prism, creating four separate spot array patterns on the detector (Figure 2). The two HyWFS analyses can be computed simultaneously without splitting light to two separate sensors, maximizing the flux on the WFS.

The images in Figure 3 are processed to appear as the output of a PyWFS or SHWFS. The HyWFS image is processed to a PyWFS image by binning the pixels to remove the separation between the spots. To process the image similar to a SHWFS, the four pupil images are linearly summed to create a single spot array (Figure 3). This single array computes the wave-front slopes by measuring the spot motion. This measurement does not require all four pupils to be illuminated. If only a single pupil is illuminated, the HyWFS will still generate a SHWFS image. The high dynamic range of the SHWFS is preserved through this process.
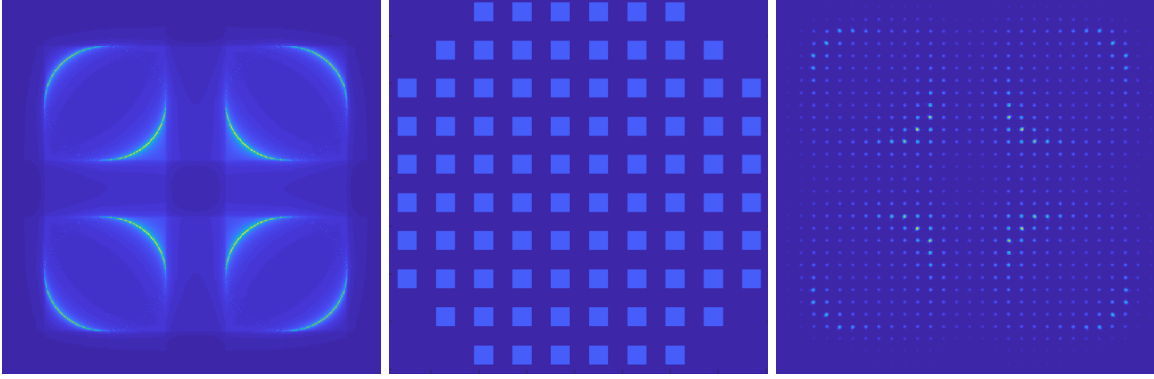
Figure 2. Left: Simulated PyWFS output using a four sided pyramid prism. Center: Simulated SHWFS output using a 10 × 10 lenslet array. Right: Simulated HyWFS output image using a four-sided pyramid prism and a 27 × 27 lenslet array
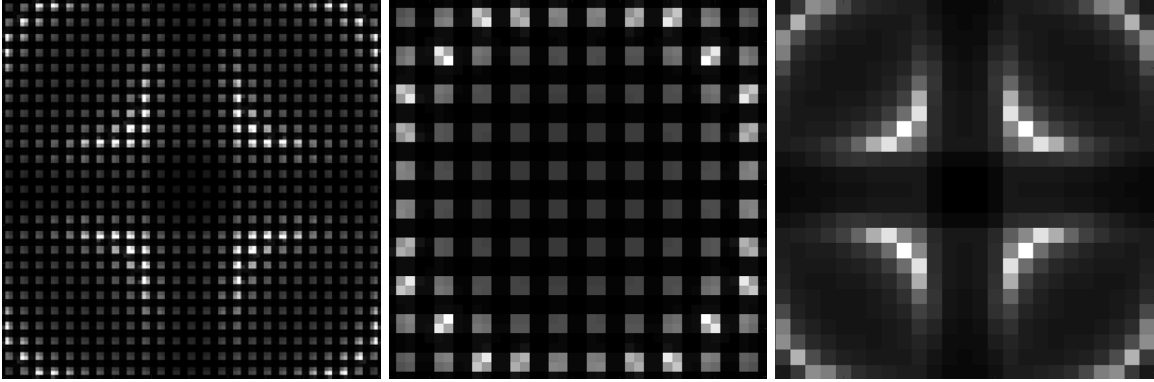

Figure 3. Left: Simulated HyWFS image with binned pixels. Center: Simulated SHWFS image processed by linearly combining intensities from the four pupils of the HyWFS image. Right: Simulated PyWFS image processed by binning the pixels to average quad cell intensities and removing the space between the focused spots.

3. RECONSTRUCTION

3.1 SHWFS Analysis

A SHWFS measures the slope of the incoming wave-front using a lenslet array. For an unaberrated wave-front, these spots are spaced equally from each other. For an aberrated wave-front, the spots shift. This shift is directly caused by the local wave-front slope over each lenslet. A SHWFS reconstructor matrix relates the spot shift to a local wave-front slope. For an unaberrated wave-front each pixel will have equal intensities. As the wave-front changes and the spots shift, the relative intensities between the pixels change. In this iteration of the HyWFS, the position is found using a centroid algorithm. The following equations represent how the spot position is found for a quad cell.

$$C_x = \frac{(I_2 + I_4) - (I_1 + I_3)}{I_1 + I_2 + I_3 + I_4}$$

$$C_y = \frac{(I_1 + I_2) - (I_3 + I_4)}{I_1 + I_2 + I_3 + I_4}$$

(1)

Known aberrations are applied to the system and their slopes are measured using Equation 1. These slope measurements are recorded in an $n \times m$ matrix where n is 2 times the number of lenslets (containing the

coordinate slope positions for each), and m is the number of applied modes. The pseudo inverse of this matrix is calculated to form the reconstructor matrix.

Once the reconstructor matrix is created, an unknown wave-front can be measured. This is done by calculating slope measurements again and recording them in a vector. This vector is multiplied by the reconstructor matrix to calculate the shape of the wave-front in terms of the known aberrations in the reconstructor.

3.2 PyWFS Analysis

In the HyWFS, a raw intensity method is used to create a PyWFS reconstruction matrix. A map of the intensity differences is calculated by using the square root of the intensity of each pixel (I) normalized by the sum from pixels in the entire image. Diffraction effects from the edge of the prism create intensity variations over the pupils. To calibrate the WFS, intensity measurements corresponding to an ideal wave-front (I_0) are subtracted from the wave-front of interest.

$$P = \frac{I_{\mathbf{x}}^{1/2}}{\sum_{\mathbf{x}} I_{\mathbf{x}}^{1/2}} - \frac{I_{0,\mathbf{x}}^{1/2}}{\sum_{\mathbf{x}} I_{0,\mathbf{x}}^{1/2}} \tag{2}$$

The rationale for the square roots in Equation 2 is that P becomes linear in the electric field amplitude at the detector. The reconstructor matrix is calibrated in the same manner as for the SHWFS, substituting the values of P for the centroids.
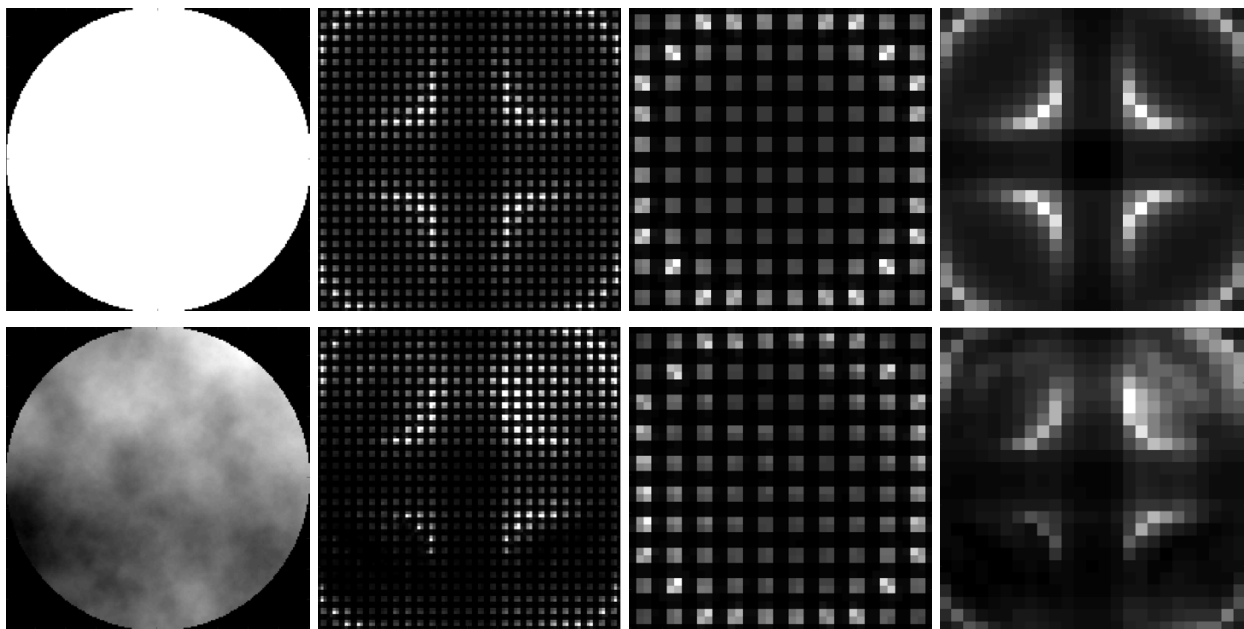

Figure 4.   Far Left: Simulated phase screen applied to the HyWFS. Left: Simulated HyWFS image resulting from the previous phase screen. Right: Simulated HyWFS image processed as a SHWFS. Far Right: HyWFS image processed as a PyWFS. Top: Ideal wave-front. Bottom: Kolmogorov phase screen.

3.3 HyWFS Reconstruction

The HyWFS image is processed as a PyWFS and as a SHWFS output image. This allows for a reconstruction of both the SHWFS and PyWFS to occur. There is a clear turning point between the SHWFS and PyWFS estimations shown as residual wave-front error after correction. Generally the system should be operating in a regime where the PyWFS reconstruction is more accurate where there are only small changes in turbulence.

Should the turbulence suddenly worsen, the HyWFS can switch to the SHWFS reconstruction simply by changing to the SHWFS estimation.

A Kolmogorov phase screen is applied to the simulated system to observe the effect on the HyWFS (Fig 4). The value of applied wave-front error (WFE) was calculated from this phase screen. There is a shift in individual spot location on the SHWFS analysis image resulting from local wave-front slopes. In the PyWFS analysis the overall tilt of the wave-front is more visible, shifting a majority of the light to the upper right pupil image. Using the previously described techniques, both the SHWFS and PyWFS processing techniques can be used to reconstruct the aberrated wave-front.

4. SIMULATION

The simulation of the HyWFS was conducted to assess the performance of the system. The simulation was tested with varying turbulence strength and photon noise to simulate the environment present during on-sky observations. The range of these variables was set to mimic possible values of a typical night sky. Photon noise was varied to test the WFS response for objects of different brightness.
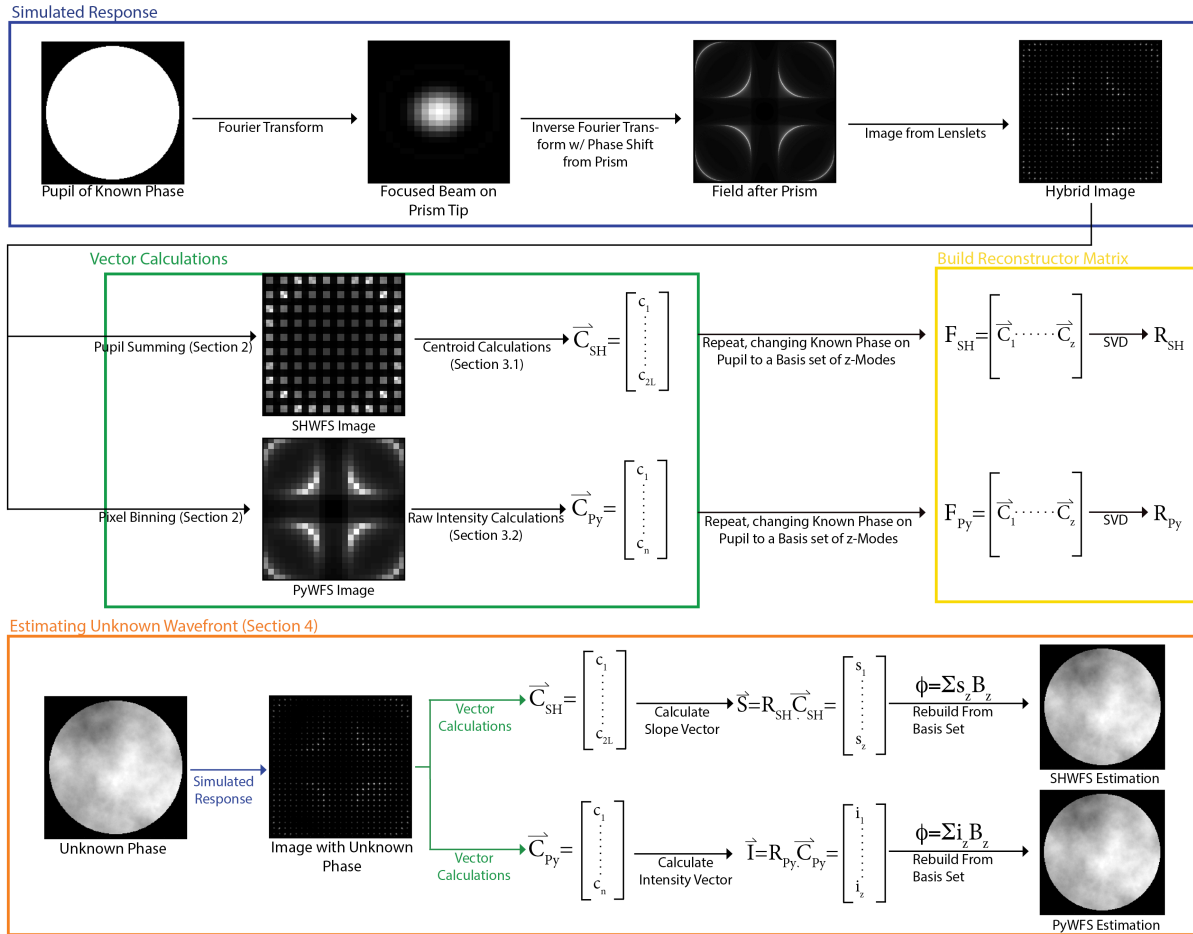

Figure 5. Diagram of wave-front estimations using the HyWFS split into four main components. Blue: The simulated response of the HyWFS. Green: Vector calculations including the image processing and slope/intensity calculations. Yellow: Building the reconstruction matrix for the HyWFS. Orange: Estimating an unknown wave-front.

4.1 Simulated HyWFS Response

Figure 5 shows the image processing chain of the HyWFS. First, the input field is simulated over the entrance pupil. For a flat wave-front (shown in diagram) there is no additional phase added. The Fourier transform of this pupil represents the image present on the tip of the pyramid prism. For a flat wave-front this will be a diffraction limited spot. The simulated design of the HyWFS consists of a four-sided pyramid prism to split a focused beam into four pupils. The prism not only splits the light, but introduces a phase shift to each side of the pupil. The field is collimated by a lens to preserve pupil size and spacing. All four pupils are incident onto a 27×27 lenslet array. The spot images created by diffraction outside the geometric pupil were ignored during the slope calculations for the SHWFS.

4.2 Building the Reconstructor Matrix

A reconstructor matrix for the HyWFS uses two separate matrices for the SHWFS and PyWFS analyses built from a basis set of Zernike polynomials. As described in Section 3, slope measurements were used to build the SHWFS reconstructor and raw intensity measurements were used for the PyWFS reconstructor shown in Figure 5 highlighted by green. The simulation applied up to the $65^t h$ Zernike polynomial to build the reconstruction matrix, shown in Figure 5 highlighted by yellow. This allows a direct comparison of the accuracy between both analysis types.

4.3 HyWFS Trials and Variables

The variable parameters for the simulations were chosen to get a more complete view of the HyWFS response. The total flux per frame was chosen between 10^3 and 10^9 photons, and the corresponding photon noise added to the final image output of the HyWFS. This range was chosen to evaluate the system performance for photon starved objects where photon noise becomes an important factor. The simulations spanned aberration strength from 3×10^{-3} to 10 radians rms, corresponding to values of D/r_0 between zero and 15. This wide range was used to explore the limits of both the SHWFS and PyWFS analyses. The PyWFS response begins to saturate when the aberration grows above ~ 1 rad rms. This is where the focused spot begins to disintegrate into a speckle pattern. The SHWFS has a much larger dynamic range, but will also saturate when local tilts begin to drive the spots into neighboring quad cells. For the system simulation it was important to model to the limit of the SHWFS.

The size of the reconstructor matrix was also varied. It was apparent that the wave-front estimates were affected by the number of Zernike modes the system attempted to correct. At low signal, the amplitudes of poorly sensed modes in the reconstructor will be estimated with signal-to-noise ratio less than one and degrade rather than improve the overall wave-front estimate. It becomes more difficult to differentiate between Zernike modes as the spatial frequency increases. To vary this, 10 reconstructor matrices were created. These matrices varied in size from 3 to 65 modes. Wave-front estimations were computed using each matrix and the most accurate was used in the final test.

4.4 HyWFS Simulation Results

The resulting wave-front estimations from the HyWFS simulations for both the SHWFS and PyWFS reconstruction are shown in Fig 6. At low flux the photon noise does not affect the PyWFS reconstruction as much as the SHWFS reconstruction. In the latter case, when the value is below 10^4 photons the residual WFE increases by an order of magnitude compared to the residual WFE of the same simulation with 10^5 photons. This noise affects the centroid calculations of the SHWFS analysis, while the effect of the noise is lessened in the PyWFS because the sensitivity is directly proportional to the diffracton limit of the telescope.

The effect of turbulence strength on the system is more dynamic. Figure 7 shows the distinct cut-off point in the PyWFS reconstruction where the estimations are no longer accurate. As expected this occurs around 1 radian rms of applied wave-front error. Below this limit the pyramid reconstruction stays consistently more accurate than the SHWFS reconstruction. The SHWFS reconstruction remains relatively linear through the saturation point of the PyWFS reconstruction, only saturating around 12 radians rms applied wave-front error.

These results show a distinct turning point in accuracy between the PyWFS and SHWFS reconstruction in response to varying turbulence.
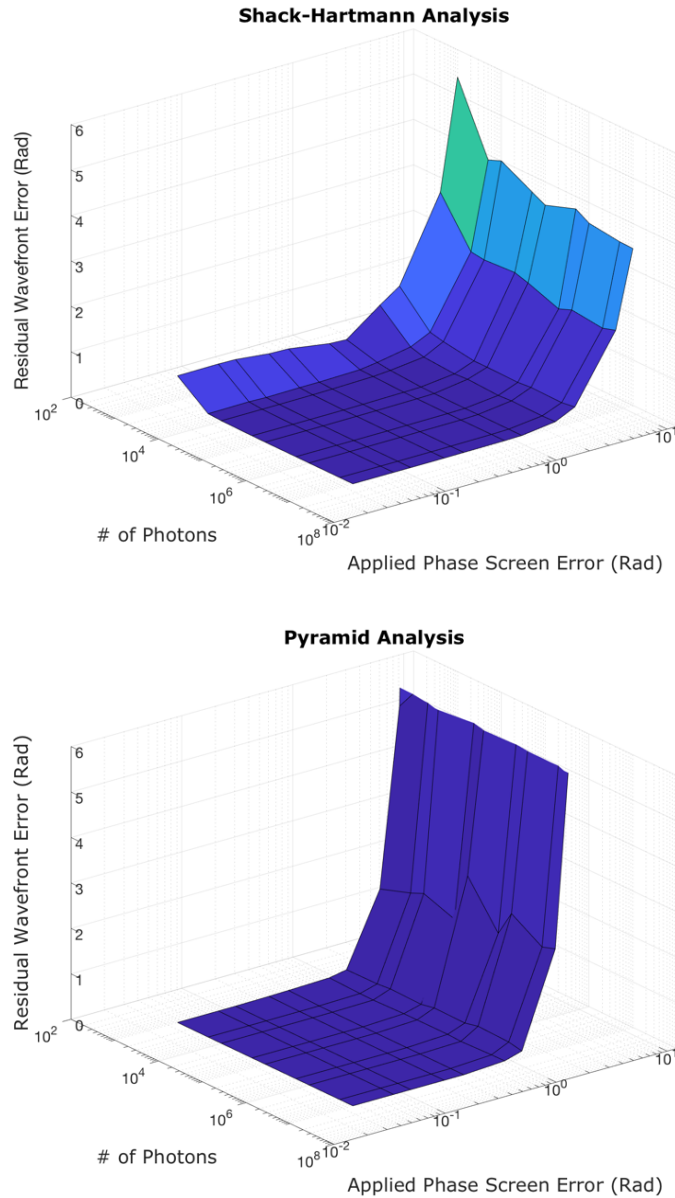
Shack-Hartmann Analysis

Pyramid Analysis

Figure 6. HyWFS trial results. Top: SHWFS analysis and reconstruction. Bottom: PyWFS analysis and reconstruction.

5. CONCLUSION AND FUTURE WORK

The HyWFS has a unique design that combines the strengths of the commonly used SHWFS and PyWFS into a single system. The system has been simulated to show the effect of varying degrees of turbulent atmosphere. In simulation the system responds as theorized, the HyWFS has both the high sensitivity of the PyWFS and high dynamic range of a SHWFS. The SHWFS reconstruction method responds well to large amplitudes of applied turbulence, while the PyWFS is highly accurate at smaller amplitude applied wave-front errors. Currently the combination allows a switch between the two reconstructions, choosing the method which better senses the incoming turbulent wave-front. Using this method the HyWFS shows that at any point it can correct as well as a typical SHWFS or PyWFS, but with the ability to switch to the one of greater accuracy.

Currently a prototype of the HyWFS has been built in a laboratory setting and is capable of taking images

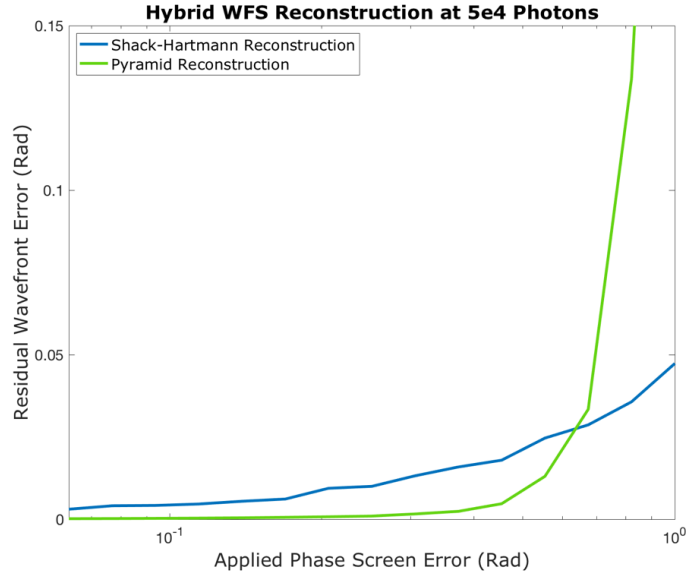**Hybrid WFS Reconstruction at 5e4 Photons**

Figure 7. Cross section of Figure 6. Turbulence strength effect on the PyWFS and SHWFS estimations. Shown is a distinct turning point in which the comparable accuracy between the two WFS switch.

similar to those shown in the simulation.[4] A future version of the HyWFS will use only a single reconstruction matrix that is more accurate than the SHWFS or PyWFS separately. Current work has shown a single reconstructor matrix that is more accurate than the SHWFS reconstruction. Ongoing work will continue to improve the single reconstruction matrix and increase the accuracy of the HyWFS.

REFERENCES

[1] Ragazzoni, R., [*Pupil plane wave sensing with an oscillating prism*], vol. 43 (1996).
[2] Chen, e. a., [*Experimental Demonstration of Sequential Operation Approach for Three-Sided Pyramid Wavefront Sensor*], vol. 8 (2016).
[3] J. L. Codona, M. Hart, L. S. M. M., [*Comparative Performance of a 3-Sided and 4-Sided Pyramid Wavefront Sensor*] (2018).
[4] Ryan Hamilton, Joseph Rice, C. G. M. H., [*Designing, Building, and Testing of a Hybrid Wavefront Sensor for Adaptive Optics*] (2019).